Opt Quant Electron (2016)48:355
DOI 10.1007/s11082-016-0601-3

# Circuit-level implementation of quantum-dot VCSEL

**M. Shekarpour[1] · K. Saghafi[1] · M. Jalali[1] · M. H. Yavari[1]**

Received: 4 February 2015 / Accepted: 13 May 2016


**Abstract** In this paper, for the first time a circuit model of quantum dot InGaAs–GaAs VCSEL including thermal effects is presented. The model is able to predict L-I characteristics for a range of ambient temperatures that the simulation results reveal a good agreement with experimental data reported in literatures. Also the effects of carrier dynamics on the QD-VCSEL performance are simulated that is accordance with results reported by other researcher. The parameters affecting high-speed optical modulation techniques, particularly on–off keying, such as turn-on delay, relaxation oscillations frequency ($f_{ro}$) and cutoff frequency for different level modulation currents are investigated. The model is compatible with circuit analysis programs.

**Keywords** Circuit model · Quantum dot (QD) · Vertical cavity surface emitting laser (VCSEL) · Thermal effect

## 1 Introduction

VCSELs in the recent years have attracted many attentions because of their relative advantages such as, low threshold current, high modulation speed and single-mode operation (Coldren and Corzine 1995; Bimberg et al. 1999; Sugawara 1999; Chuang 2009; Xu et al. 2008; Abbaspour et al. 2011). Their applications are expanded beyond the optical communication systems toward the optical interconnects and optical signal processing systems (Wilmsen et al. 1999). In addition, the promising quantum dot structure can yield

✉ K. Saghafi
saghafi@shahed.ac.ir

[1] Electrical Engineering Department, Shahed University, Tehran, Iran

Published online: 17 June 2016

high thermal stability, improved dynamic characteristics and higher material gain (Ledentsov 2002; Yavari and Ahmadi 2011). However, the main drawbacks of the VCSEL are strong thermal dependent behavior and the polarization instabilities. The effects such as increased noise and bistability of lasing modes are due to the absence of a well-defined polarization selection mechanism affected by thermal dependent behavior (Michalzik 2013; Masoller and Torre 2008). Consequently, VCSEL models must account for thermal effects. Numerical models are mostly accurate but very complicated and heavy to calculate. Circuit models, on the other hand, are less accurate while highly suitable for computer-aided analysis of optoelectronic systems that include electronic circuits and photonic components. Some circuit models for various types of lasers are developed based on one-level rate equations (Lu et al. 1995a, b; Nguyen et al. 1995; Mena et al. 1999). However, since the interaction between all layers are not considered well when using one-level rate equations, the model cannot adequately cover high-speed effects (Tsou and Pulfrey 1997). Other models that utilize multi-level rate equations usually ignored to include the thermal effects (Shastri et al. 2011; Yavari and Ahmadi 2009). In this paper, to our knowledge, for the first time a QD-VCSEL circuit model based on the multi-level rate equation by considering thermal effects is implemented.

In Sect. 2, the QD-VCSEL rate equations are presented. Circuit model implementation including thermal effects is described in Sect. 3. Section 4 demonstrates simulation results that includes transient response, eye diagram, steady-state and modulation response. Finally, the paper is concluded in Sect. 5.

## 2 Rate equations

The active region energy band diagram of a InGaAs–GaAs QD-VCSEL is shown in Fig. 1. To implement QD-VCSEL circuit model, we modified the standard QDL rate equations by considering experimental QD-VCSEL parameters, specifically relaxation times, to math QD-VCSEL behavior.The rate equations including carrier transport, relaxation, capture and escape processes in the cladding layer, quantum well (QW) or wetting layer (WL) and QDs layers are given by,

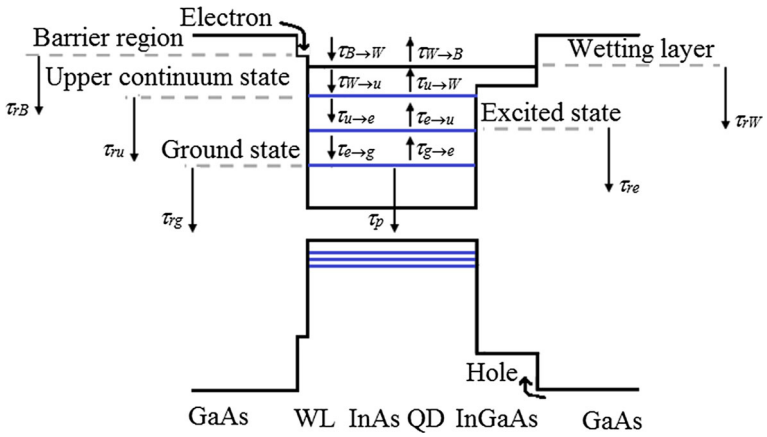


**Fig. 1** Energy band diagram of the active region of the self-assembled InGaAs–GaAs QD-VCSEL

$$\frac{dN_B}{dt} = \frac{\eta_i I}{q} + \frac{N_W}{\tau_{W\to B}} - \frac{N_B}{\tau_{B\to W}} - \frac{N_B}{\tau_{rB}} \tag{1}$$

$$\frac{dN_W}{dt} = \frac{N_B}{\tau_{B\to W}} - \frac{N_W}{\tau_{W\to B}} + \frac{N_u}{\tau_{u\to W}} - \frac{N_W}{\tau_{W\to u}} - \frac{N_W}{\tau_{rW}} \tag{2}$$

$$\frac{dN_u}{dt} = \frac{N_W}{\tau_{W\to u}} - \frac{N_u}{\tau_{u\to W}} + \frac{N_e}{\tau_{e\to u}} - \frac{N_u}{\tau_{u\to e}} - \frac{N_u}{\tau_{ru}} \tag{3}$$

$$\frac{dN_e}{dt} = \frac{N_u}{\tau_{u\to e}} - \frac{N_e}{\tau_{e\to u}} + \frac{N_g}{\tau_{g\to e}} - \frac{N_e}{\tau_{e\to g}} - \frac{N_e}{\tau_{re}} \tag{4}$$

$$\frac{dN_g}{dt} = \frac{N_e}{\tau_{e\to g}} - \frac{N_g}{\tau_{g\to e}} - \frac{N_g}{\tau_{rg}} - \frac{v_g g_m (2P_g - 1)}{1 + \varepsilon S} S \tag{5}$$

$$\frac{dS}{dt} = \frac{v_g g_m (2P_g - 1)}{1 + \varepsilon S} S - \frac{S}{\tau_p} \tag{6}$$

In these equations, $N_B$, $N_W$, $N_u$, $N_e$ and $N_g$ are carrier numbers in the barrier region, wetting layer, upper continuum state, excited state, and ground state respectively, $\eta_i$ is the injection efficiency, $I$ denotes the injected current and $S$ stands for the photon number. The total carrier transport time from cladding layer into QW or WL is $\tau_{B\to W} = \tau_r + \tau_c$ (Zory et al. 1993; Schneider and Klitzing 1988), where $\tau_c$ is the carrier capture time of QW or WL and $\tau_r$ is the carrier transit time from the cladding layer to QW or WL defined as $\tau_r = L_s^2/2D_{n,p}$ ($L_s$ is the distance from the doped cladding layer to the QW, $D_n$ and $D_p$ are diffusion coefficients of electrons and holes, respectively, defined by $D_{n,p} = (k_B T/q)\mu_{n,p}$). The thermionic emission time in the QW or WL is expressed as (Schneider and Klitzing 1988)

$$\tau_{W\to B} = L_W \left[\frac{2\pi m^*}{k_B T}\right]^{1/2} \exp\left(\frac{E_{bW}}{k_B T}\right) \tag{7}$$

where, $L_W$, $m^*$ and $E_{BW}$ denote the width of the QW or WL, effective mass and the effective energy barrier, respectively. The relaxation rate from the wetting layer to the upper continuum state is (Sugawara et al. 2005)

$$\tau_{W\to u}^{-1} = (1 - P_u)\tau_{W\to u,0}^{-1} \tag{8}$$

where

$$P_u = \frac{N_u}{2N_D V_a} \tag{9}$$

represents the occupation of the continuum state ($\tau_{W\to u,0}^{-1}$ is the relaxation rate when $P_u = 0$). $N_D$ and $V_a$ denote quantum volume density and active region volume. The relaxation rate from the upper continuum state to the wetting layer is (Sugawara et al. 2005)

$$\tau_{u\to W}^{-1} = \left(1 - \frac{N_W}{2D_W}\right)\tau_{u\to W,0}^{-1} \tag{10}$$

where $\tau_{u\to W,0}^{-1}$ is the rate when $N_W = 0$ and $D_W$ denotes the degeneracy of the wetting layer. The relaxation rate from the upper continuum state to the excited state is (Sugawara et al. 2005)

$$\tau_{u\to e}^{-1} = (1 - P_e)\tau_{u\to e,0}^{-1} \tag{11}$$

where

$$P_e = \frac{N_e}{2N_D V_a} \tag{12}$$

represents the occupation of the excited state($\tau_{u\to e,0}^{-1}$ is the relaxation rate when $P_e = 0$). The excitation rate is

$$\tau_{e\to u}^{-1} = (1 - P_u)\tau_{e\to u,0}^{-1} \tag{13}$$

where $\tau_{e_{\to u,0}}^{-1}$ is the rate when $P_e = 0$. The relaxation rate from the excited state to the ground state is

$$\tau_{e\to g}^{-1} = (1 - P_g)\tau_{e\to g,0}^{-1} \tag{14}$$

where

$$P_g = \frac{N_g}{2N_D V_a} \tag{15}$$

represents the occupation of the ground state ($\tau_{e\to g,0}^{-1}$ is the relaxation rate when $P_g = 0$). The excitation rate is (Sugawara et al. 2005)

$$\tau_{g\to e}^{-1} = (1 - P_e)\tau_{g\to e,0}^{-1} \tag{16}$$

where $\tau_{g\to e,0}^{-1}$ is the relaxation rate when $P_e = 0$. The relationship between the relaxation and emission rates of carriers as

$$\tau_{g\to e,0} = (D_g/D_e)\tau_{e\to g,0}\exp(\Delta E_{eg}/kT) \tag{17}$$

$$\tau_{e\to u,0} = (D_e/D_u)\tau_{u\to e,0}\exp(\Delta E_{ue}/kT) \tag{18}$$

where $k$ is the Boltzmann constant and $T$ is temperature. $D_g = 1$, $D_e = 3$ and $D_u = 10$ are the degeneracy of the energy states. Also $\Delta E_{eg} = 70$ meV and $\Delta E_{ue} = 70$ meV are the energy separation between the ground and excited state, and between the excited state and the upper continuum state (Sugawara et al. 2005). $g_m$ in Eq. (5) and Eq. (6) is the maximum modal gain described as (Tong et al. 2006)

$$g_m = \frac{\hbar q}{cn_r m_0 \varepsilon_0}\frac{|p_{cv}|^2}{m_0 E_L}\sqrt{2\pi}\left(\frac{2.35}{F_{in}}\right)\frac{\Gamma\rho}{d_D} \tag{19}$$

where, $\hbar$, $q$, $c$ $n_r$, $m_0$, $\varepsilon_0$ and $E_L$ are the Planck's constant, electronic charge, velocity of light, refractive index of the active region, electron rest mass, absolute permittivity in vacuum, and lasing energy, respectively, $|P_{cv}|^2 = 2m_0 E_L$ for InGaAs QDs (Sugawara 1999), $d_D$ is the thickness of one QD layer, $\Gamma$ is the optical confinement factor, and $F_{in}$ is the full-width at half-maximum (FWHM) of the inhomogeneous broadening of the QDs. In

Eq. (6), $\varepsilon = \varepsilon_m \Gamma / V_a$, in which $\varepsilon_m$ is the nonlinear gain coefficient expressed as (Sugawara 1999)

$$\varepsilon_m = \frac{q^2}{c n_r^2 m_0 \varepsilon_0} \frac{|p_{cv}|^2}{m_0 E_L} \frac{1}{F_{ho}} t_p \tag{20}$$

where $2\hbar F_{ho}$ is the FWHM of the homogeneous broadening of the QDs lasing spectra. The material and geometrical parameters utilized in the proposed circuit model of the QD-VCSEL are tabulated in Table 1.

## 3 Circuit model including thermal effects

Without considering thermal effects, the rate equations Eqs. (1)–(6) tend to display a smooth uprising behavior for output optical power in respect to injection current as shown in Fig. 2. In reality, at moderate currents the slope of the L-I curve gradually diminishes until at high currents that roll over occurs. To develop a circuit model including these thermal effects we need to determine a method including these effects valid for static and dynamic analysis. A solution is to write the main VCSEL parameters as functions of temperature (Yu et al. 1996; Byrne and Keating 1989). However, in this way numerical solutions are preferred because of the complexity and lots of details. An efficient way suitable for circuit modeling, as shown in Fig. 2, is to define a temperature dependent modifying current $\Delta I(T)$ to be subtracted from the main injection current resulting in a lower optical power and thus reduction of the slope of the L-I curve. As an approximation, $\Delta I(t)$ can be defined by the following polynomial (Mena et al. 1999):

**Table 1** Parameters used in QD-VCSEL circuit model (Tong et al. 2006, 2009a; Zory et al. 1993; Schneider and Klitzing 1988; Sugawara et al. 2005)

| Symbol | Description | Value |
|---|---|---|
| $\tau_c$ | Carrier capture time | 0.3 ps |
| $\tau_{W\to u,0}$ | Carrier relaxation lifetime from WL to the upper continuum state | 1 ps |
| $\tau_{u\to W,0}$ | Carrier escape time from upper continuum state to WL | 10 ps |
| $\tau_{u\to e,0}$, $\tau_{e\to g,0}$ | Carrier relaxation lifetime | 3.4 ps |
| $\tau_{ri(i=B,\ W,\ u,\ e,\ g)}$ | Recombination lifetime | 1 ns |
| $\tau_p$ | Photon life time in the cavity | 4.75 ps |
| $L_s$ | Distance from the doped cladding layer to QW | 0.2 μm |
| $E_{BW}$ | Effective energy barrier | 102 meV (electron)<br>93 meV (hole) |
| $V_a$ | Active region volume | $1.5 \times 10^{-17}$ m$^3$ |
| $N_D$ | QD volume density | $8.33 \times 10^{22}$ m$^{-3}$ |
| $V_D$ | Volume of one QD | $1.6 \times 10^{-24}$ m$^3$ |
| $\rho$ | QD surface density | $5 \times 10^{+10}$ cm$^{-2}$ |
| $\Gamma$ | Optical confinement factor | 0.06 |
| $n_r$ | Refractive index | 3.5 |
| $\tau_{th}$ | Thermal time constant | 1 μs |

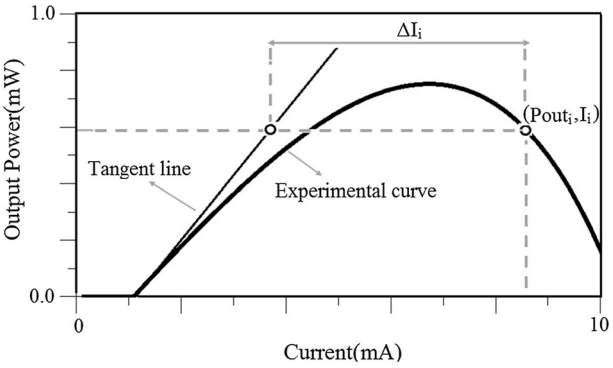


**Fig. 2** Determine four points on the L-I curve for extract offset current parameters

$$\Delta I(T) \approx a_0 + a_1 T + a_2 T^2 + a_3 T^3 \tag{21}$$

where $a_0$–$a_3$ are constant coefficients. By proper defining the internal temperature, $T$, and constant coefficients this method can also predict the roll-over effect at high modulation currents as well.

To start the modelling procedure, we need an expression to calculate the device internal temperature as a function of ambient temperature, $T_0$, and device self heat up. It will be assumed that the difference between input electrical power $P_{in}$ and output optical power $P_{out}$ is dissipated as heat (Yu et al. 1996; Bewtra et al. 1995). So

$$T = T_0 + (P_{in} - P_{out})R_{th} - \tau_{th}\frac{dT}{dt} \tag{22}$$

where $P_{in} = IV$ and $I$ and $V$ denote the injection current and over dropped voltage of the laser, respectively, $R_{th}$ is defined as the VCSEL's thermal impedance and $\tau_{th}$ is the device thermal time constant.

Another important aspect of implementing the circuit model, is to determine a temperature dependent current–voltage (IV) characteristic of the device. It can be written either in forms of a diode-like relationship or a polynomial functions of current and temperature (Mena et al. 1999). The advantages of the polynomial is its simplicity and the ability of accurate prediction of the voltage by defining its dependence to injection current and internal temperature as follows

$$\begin{aligned} V &= f(T)g(I) \\ &= (b_0 + b_1 T + b_2 T^2 + \cdots)(c_0 + c_1 I + c_2 I^2 + \cdots) \end{aligned} \tag{23}$$

where $b_0$–$b_n$ and $c_0$–$c_n$ are constant parameters obtained from experimental data. To implement the rate equation in the simulator for using in photonic and optoelectronic system design, the circuit model must be able to be connected to electrical parts such as driver and transmitter. Therefore it is required to transform physical and optical quantities to circuit parameters. The carrier numbers $N_i$ ($i = B, W, u, e, g$) can be transformed to node voltages $V_i$ assuming they are charges on a capacitor $C_i$ with an arbitrary value such that $qN_i = c_i V_i$. In addition, photon numbers $S$ can also be transformed to a node voltage. However, since node voltages can acquire a negative value, there is a risk that output optical power $P_{out} = kS$ becomes negative. So, we define $P_{out} = (V_p + \delta)^2$, where $V_p$ is

the corresponding node voltage and $\delta$ is a small arbitrary constants (Mena et al. 1997). After substituting these transformations into Eqs. (2)–(6), the equivalent circuit is obtained as shown in Fig. 3.

Figure 3a represents input electrical terminals of QD-VCSEL that receives incoming current $I_{in}$ and results over drop voltage $V$ according to Eq. (22) by means of $E_{in}$ as a non-linear voltage source. The injection current is $I = I_{in} - C_{in}\, d(V_{in} - I_{in}R_S)/dt$ where $C_{in}$ stands for all parasitic capacitances and $R_S$ represents series parasitic resistance.

Based on Eq. (1) the circuit model of the barrier layer is depicted in Fig. 3b where $R_B = \eta_i \tau_{rB}/c_i$, $C_B = c_i/\eta_i$, and as current sources $G_{B\to W} = V_B c_i/\tau_{B\to W}\ \eta_i$, and $G_{W\to B} = V_B c_i/t_{W\to B}\eta_i$. Temperature effects are modelled by $G_{off} = \Delta I(T)$ and the node voltage $V_B$ implicitly represents carrier numbers in the layer. In Fig. 3c wetting layer carrier number is modelled by $V_W$ where $R_W = \tau_{rW}/c_i$, $C_W = c_i$, $G_{W\to u} = V_W c_i/\tau_{W\to u}$, $G_{u\to W} = V_W c_i/\tau_{u\to W}$ and the current sources $G_{B\to W}$ and $G_{W\to B}$ stand for carrier interaction with barrier layer. Using a same process, the second and first exited states are model as given in Fig. 3d, e where $R_u = \tau_{ru}/c_i$, $C_u = c_i$, $G_{u\to e} = V_u c_i/\tau_{u\to e}$ $G_{e\to u} = V_e c_i/\tau_{e\to u}$ and $R_e = \tau_{re}/c_i$, $C_e = c_i$, $G_{e\to g} = V_e c_i/\tau_{e\to g}$ for state of upper and exited respectively. Figure 3f models the ground state using the $R_g = \tau_{rg}/c_i$, $C_g = c_i$, $G_{e\to g} = V_e c_i/\tau_{e\to g}$, $G_{g\to e} = V_g c_i/\tau_{g\to e}$ and the current sources $G_{STn}$ with the following value

$$G_{STn} = \frac{q v_g g_m}{k} \frac{\left(\frac{c_i V_g}{q N_D V_a} - 1\right)}{1 + \frac{\varepsilon}{k}(V_p + \delta)^2} (V_p + \delta)^2. \tag{24}$$

Using the circuit in Fig. 3g, the internal temperature of the device is simulated according to Eq. (22) as a node voltage $V_T$ to be used in $E_{in}$ and $G_{off}$ in Fig. 3a, b affecting V-I and L-I characteristics, respectively, where we have $R_T = R_{th}$, $C_T = \tau_{th}/R_{th}$ and $G_T = T_0/R_{th} + (P_{in} - P_{out})$. Finally, the output optical power of the device $P_{out}$ is produced in Fig. 3h where we have $E_{po} = (V_P + \delta)^2$. The photon rate equation is modelled with the resistance $R_{ph} = 1$, capacitance $C_{ph} = 2\tau_p$ and $G_{STm}$ defined as

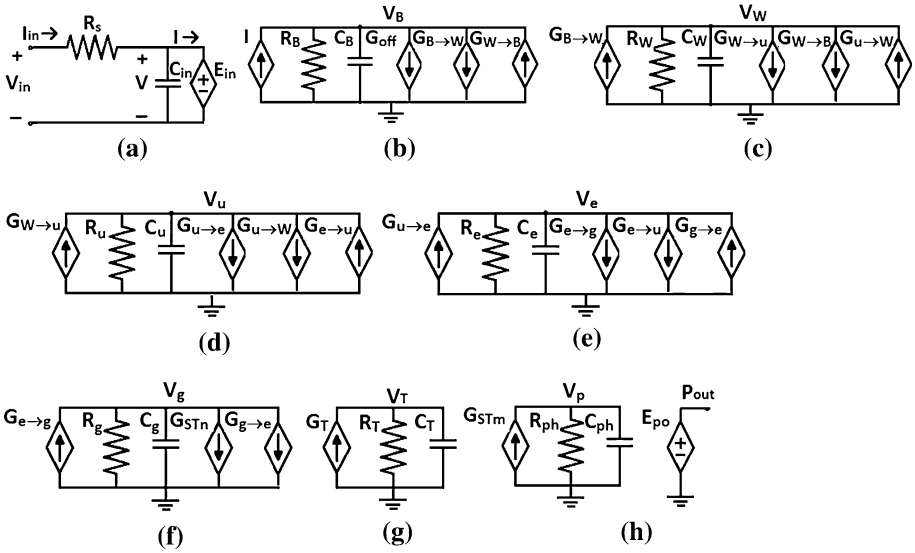


**Fig. 3** Equivalent-circuit implementation of QD-VCSEL model

$$G_{STm} = \frac{v_g g_m \left(\frac{c_i V_g}{qN_D V_a} - 1\right)(V_p + \delta)}{1 + \frac{\varepsilon}{k}(V_p + \delta)^2} - \delta. \tag{25}$$

## 4 Simulation results of the circuit model

The proposed circuit model is able to demonstrate the effect of internal parameters of the QD-VCSEL such as change of carrier relaxation lifetime, recombination lifetime and inhomogeneous broadening on output light power.

To deal with the thermal behaviour of L-I curve, the constant parameters in the polynomial representing $\Delta I(T)$ should be obtained well. The method to extract these parameters from experimental curves is as follows. First, a tangent line to the experimental L-I curve at the threshold point is plotted. In fact this line with the slope of the tangent to the main L-I curve would be the circuit model response if thermal effects not considered. We have assumed $\Delta I(T)$ has a third order behaviour. Noted that the order can be selected higher at the expense of higher volumes of calculations. To calculate $a_0$–$a_3$, we need to specify at least four points on the curve and calculate the corresponding $\Delta I_i$ as the space between the main curve and the tangent line (see Fig. 2). Note that to account for the effect of the roll-over, one or two points must be chosen after the place that the maximum power reached. For each point the corresponding internal temperature should also be defined as $T_i = -T_0 + (I_i V_i - P_{outi})R_{th}$, according to Eq. (22) where $V_i$ and $P_{outi}$ come from VI and L-I curves, respectively. Since the analysis is carried out in static mode we have dT/dt = 0. Now by solving four equations as $a_0 + a_1 T_i^1 + a_2 T_i^2 + a_3 T_i^3 = \Delta I_i$, $a_0$–$a_3$ will be achieved.

The process mentioned thus far, is repeated for different values of $R_{th}$. Eventually the one that more matched the experimental data is selected. The results obtained for a self-assembled InGaAs–GaAs QD VCSEL laser using the experimental L-I and VI curves provided in Yu et al. (1996) and Byrne and Keating (1989) are as follows: $a_0 = -5.01347\text{e}{-4}$, $a_1 = -4.58713\text{e}{-006}$, $a_2 = 3.3865\text{e}{-008}$, $a_3 = 4.83053\text{e}{-010}$ and $R_{th} = 1\text{e}4$.

The LI curve as a static characteristic, exhibits the laser output power versus modulation current for different temperature ranges. Figure 4 shows results obtained from the proposed circuit model expressing a good agreement with the experimental data when compared with the measured results given in (Tong et al. 2009b). Noted that the experimental results for 55 and 65 °C were not available. According to the results, by increasing the temperature, the threshold current increases and the output optical power decreases. Also, the roll-over phenomenon will occurred in lower modulation currents.

As explained in Sect. 2, multi-level rate equation is used to obtain the QD-VCSEL circuit model including upper and excited states. To show the importance of excited states on the laser performance, Figs. 5 and 6 show the static and dynamic analysis by and without considering the excited states (ES's). According to the DC analysis shown in Fig. 5a, considering the ES's leads to increasing the threshold current and decreasing the output power. Also, carrier numbers are compared in Fig. 5b. $n_{g1}$ and $n_{w1}$ show carrier numbers in the case of ignoring ES's and $n_{g2}$, $n_{e2}$, $n_{u2}$ and $n_{w2}$ show carrier numbers in the case of considering excited states. Obviously, carrier numbers will be over estimated if some one ignores ES's. Transient response is shown in Fig. 6. Settling time is increased and relaxation oscillation (RO) frequency is decreased by considering the excited states.

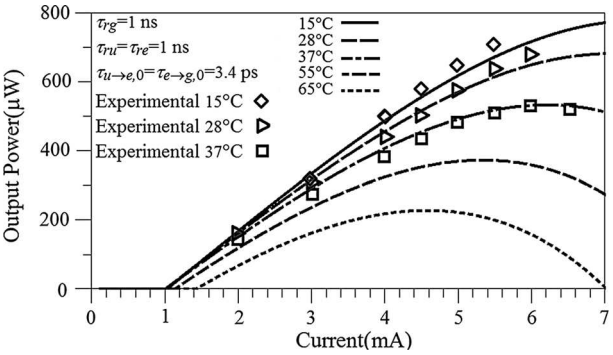


**Fig. 4** Comparison between experimental data (Tong et al. 2009b), and circuit model results simulation for different ambient temperature

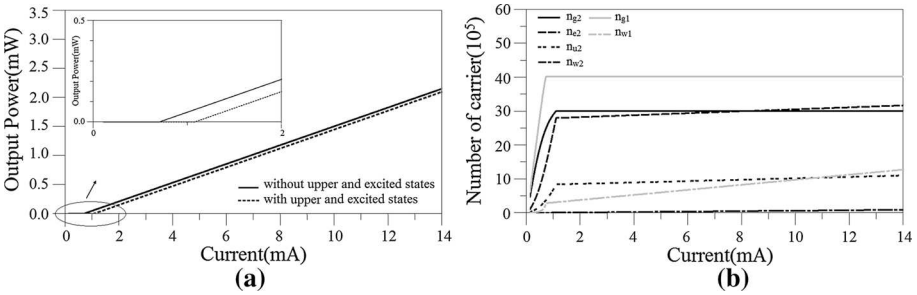


**Fig. 5** The static analysis by and without considering the excited states (ES's). **a** L-I curves. **b** Carrier numbers for different states

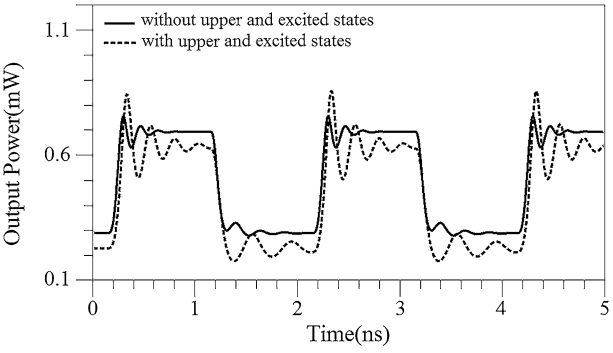


**Fig. 6** Transient response by and without considering the excited states (ES's)

Consequently, taking into account the detail of excited state dynamics are important to exactly estimate the maximum bit rate and modulation bandwidth of QDL.

Figure 7a shows the laser optical response to modulated injection current (swings from $1.5I_{th}$ to $3I_{th}$) for different relaxation times ($\tau_{u\to e,0}$,$\tau_{e\to g,0}$). by increasing the relaxation

time, the relaxation oscillation is damped and the output power decreases, that is due to the degradation of external quantum efficiency. Also the transient response for different temperatures is shown in Fig. 7b. According to the L-I characteristics for different temperatures, the increase of temperature leads to decreases the output power of laser.

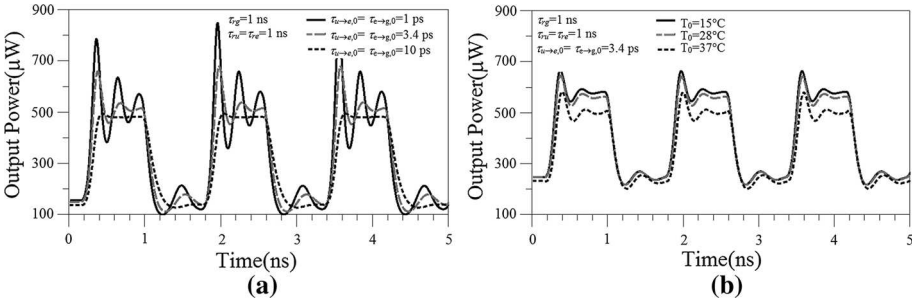


**Fig. 7** Transient response. **a** With $\tau_{ru} = \tau_{re} = \tau_{rg} = 1$ ns for different relaxation times: $\tau_{u\to e,0} = \tau_{e\to g,0} = 1,3.4,10$ ps. **b** With $\tau_{ru} = \tau_{re} = \tau_{rg} = 1$ ns and $\tau_{u\to e,0} = \tau_{e\to g,0} = 3.4$ ps for different temperature

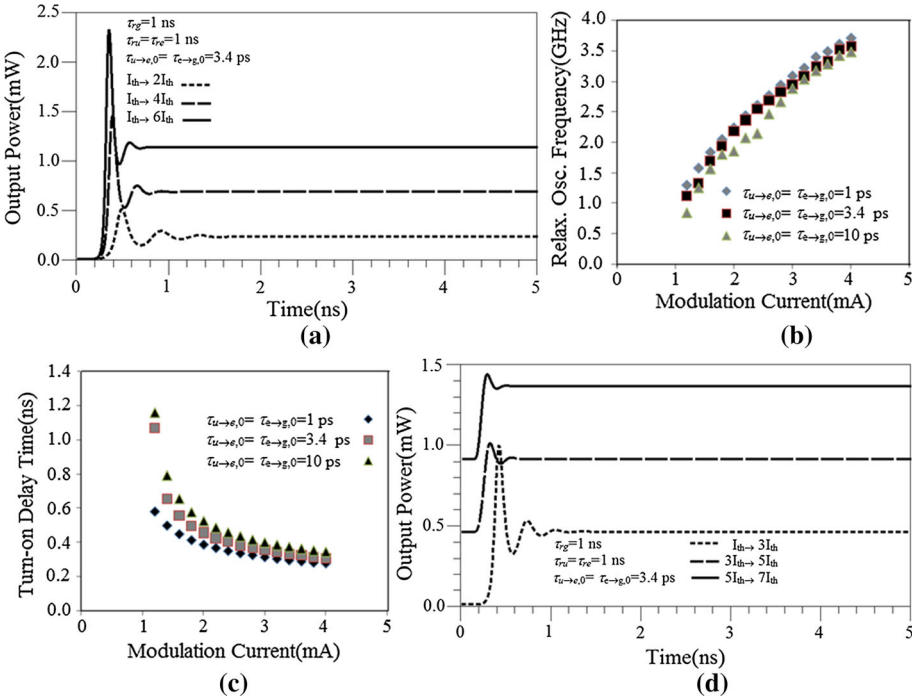


**Fig. 8** Effect of current level. **a** Step response of the injection current for a fixed primary level of $I_{th}$ and various secondary levels of $2I_{th}$, $4I_{th}$ and $6I_{th}$. **b** Relaxation oscillations frequency ($f_{ro}$) versus modulation current for relaxation times as a parameter. **c** Turn-on delay versus modulation currents for relaxation times as a parameter. **d** Step response of QD-VCSEL for different initial current levels ($I_{th}$, $3I_{th}$ and $5I_{th}$) and a constant difference between the low and high levels ($2I_{th}$)

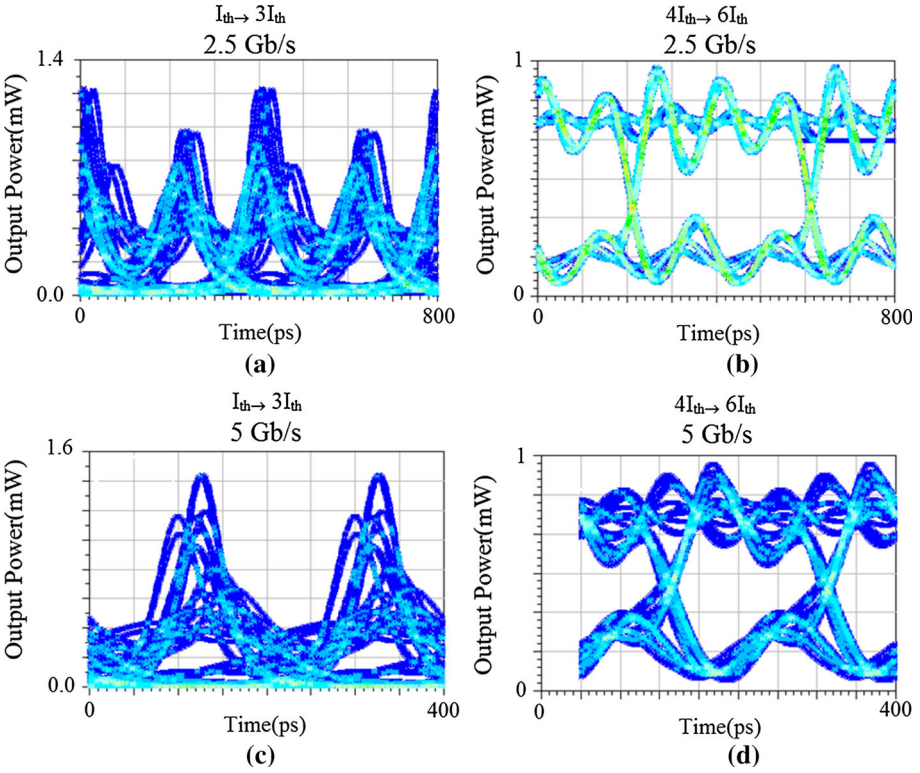


**Fig. 9** Eye diagram for two different frequencies of 2.5 and 5 Gb/s and two input current pulse levels. **a** For 2.5 Gb/s and current level of $I_{th} \rightarrow 3\ I_{th}$. **b** For 2.5 Gb/s and current level of $4\ I_{th} \rightarrow 6\ I_{th}$. **c** For 5 Gb/s and current level of $I_{th} \rightarrow 3\ I_{th}$. **d** For 5 Gb/s and current level of $4\ I_{th} \rightarrow 6\ I_{th}$

For time domain analysis, some behaviours observed in step response such as turn-on delay, overshoot, relaxation time and frequency of relaxation oscillations should to be investigated. In addition, for different levels of injection current, to measure the maximum bit rate that the laser can support, it is required to analyse the eye diagram in response to a random bit stream. Figure 8a shows the step response of the injection current for a fixed primary level of $I_{th}$ and various secondary levels of 2 $I_{th}$, 4 $I_{th}$ and 6 $I_{th}$. As can be seen, with increasing the value of the secondary level, the frequency of relaxation oscillations, $f_{ro}$, increases while the relaxation time as a limiting factor of modulation speed will be reduced. Figure 8b shows that how $f_{ro}$ changes in respect to various values of the injection current. A square root behaviour can be observed as $f_{ro} \propto (I_{mod} - I_{th})^{0.5}$. In other words, as the injected current levels goes high, the generated photon density will be increased leading to a high oscillation frequency (Shchukin et al. 2008). Relaxation time and turn-on delay are also crucial in determining the maximum achievable bit rate. Figure 8c shows the values of turn-on delay for different values of $I_{mod}$. Approximately, turn-on delay is proportional to $t_{delay} \propto 1/I_{mod}$ (Lüdge et al. 2008). Turn-on delay decreases by increasing the modulation current. The results obtained from circuit model in Fig. 8b,c are accordance with (Lüdge et al. 2008). So higher laser modulation current is demanded in high speed optical communication systems.

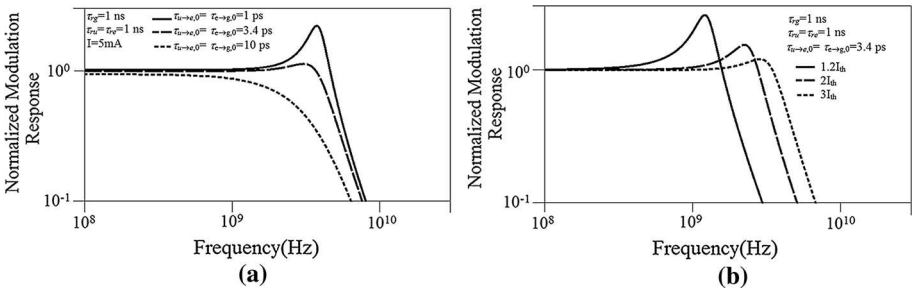


**Fig. 10** Modulation response of the QD laser. **a** With $\tau_{ru} = \tau_{re} = \tau_{rg} = 1$ ns, $I_{bias\ current} = 5$ mA and different carrier relaxation lifetime $\tau_{u\to e,0} = \tau_{e\to g,0} = 1,3.4,10$ ps. **b** For the different bias currents

The step response for a constant pulse height but different initial levels of $I_{th}$, $3I_{th}$ and $5I_{th}$ are shown in Fig. 8d. Obviously, by increasing the initial bias level the overshoot, relaxation time and turn on delay will be decreased. Thus, there might be a tendency towards higher modulation currents. However, this can lead to a higher power consumption thus overheating the laser and higher risk of damage.

The eye diagram for 2.5 and 5 Gb/s bit-rates at two different input current pulse levels of $I_{th} \rightarrow 3I_{th}$ and $4I_{th} \rightarrow 6I_{th}$ are plotted in Fig. 9. The eye is more open with raising the current levels. This is mainly due to the reduction of peak overshoot and relaxation time that is accordance with Lüdge et al. (2010). In other words, the higher initial current leads to, the higher data rate. However, increasing the modulation current levels will compromise required between power consumption (laser heating) and the cutoff frequency. The effects of different relaxation time and bias current on the small-signal frequency response are depicted in Fig. 10a, b respectively. The amplitude of modulation current is considered to be less than one percent of bias current. Results of Fig. 10a show that the high cutoff frequency occurs in lower relaxation time. As can be seen in Fig. 10b, at higher bias current, cutoff frequency is shifted to higher values. Thus increasing the pump current enhances the frequency response.

## 5 Conclusion

A circuit model based on the multi-level rate equations for QD-VCSEL that includes thermal effects is developed. A temperature dependent modified current equation is defined to import thermal effects into the rate equations. The results show this model is useful for simulating the QD-VCSEL thermal L-I characteristic and capable to predict rollover effect at high injection currents. In addition this model can simulate the carrier dynamic effects on the threshold current, external quantum efficiency, and output power. Also, with the proposed circuit model, we can evaluated the required injection current levels to reach a specific modulation speed by investigating the relaxation oscillation, turn-on delay and cut-off frequency.

## References

Abbaspour, H., Ahmadi, V., Yavari, M.H.: Analysis of QD VCSEL dynamic characteristics considering homogeneous and inhomogeneous broadening. IEEE J. Sel. Top. Quantum Electron. **17**(5), 1327–1333 (2011)

Bewtra, N., Suda, D.A., Tan, G.L., Chatenoud, F., Xu, J.M.: Modeling of quantum-well lasers with electro-opto-thermal interaction. IEEE J. Sel. Top. Quantum Electron. **1**(2), 331–340 (1995)
Bimberg, D., Grundmann, M., Ledenstov, N.N.: Quantum Dot Heterostructures. Wiley, New York (1999)
Byrne, D.M., Keating, B.A.: A laser diode model based on temperature dependent rate equations. IEEE Photonics Technol. Lett. **1**(11), 356–359 (1989)
Chuang, S.L.: Physics of Photonic Devices. Wiley, New York (2009)
Coldren, L.A., Corzine, S.W.: Diode Lasers and Photonic Integrated Circuits. Wiley, New York (1995)
Ledentsov, N.N.: Long-wavelength quantum-dot lasers on GaAs substrates: from media to device concepts. IEEE J. Sel. Top. Quantum Electron. **8**(5), 1015–1024 (2002)
Lu, M.F., Deng, J.S., Juang, C., Jou, M.J., Lee, B.J.: Equivalent circuit model of quantum well lasers. IEEE J. Quantum Electron. **31**(8), 1418–1422 (1995a)
Lu, M.F., Juang, C., Jou, M.J., Lee, B.J.: Study of carrier transport effects on quantum well lasers using a SPICE simulator. Proc. Inst. Elect. Eng. Optoelectron. **142**, 237–240 (1995b)
Lüdge, K., Bormann, M.J.P., Malić, E., Hövel, P., Kuntz, M., Bimberg, D., Knorr, A., Schöll, E.: Turn-on dynamics and modulation response in semiconductor quantum dot lasers. Phys. Rev. B **78**(3), 035316 (2008)
Lüdge, K., Aust, R., Fiol, G., Stubenrauch, M., Arsenijevic, D., Bimberg, D., Schöll, E.: Large-signal response of semiconductor quantum-dot lasers. IEEE J. Quantum Electron. **46**(12), 1755–1762 (2010)
Masoller, C., Torre, M.S.: Modeling thermal effects and polarization competition in vertical-cavity surface-emitting lasers. Opt. Express **16**(26), 21282–21296 (2008)
Mena, P.V., Kang, S.M., DeTemple, T.A.: Rate-equation-based laser models with a single solution regime. J. Lightwave Technol. **15**(4), 717–730 (1997)
Mena, P.V., Morikuni, J.J., Kang, S.M., Harton, A.V., Wyatt, K.W.: A Simple rate-equation-based thermal VCSEL model. J. Lightwave Technol. **17**(5), 865–872 (1999)
Michalzik, R.: VCSELs-Fundamentals, Technology and Applications of Vertical-Cavity Surface-Emitting Lasers. Springer, Berlin (2013)
Nguyen, L.V.T., Lowery, A.J., Gurney, P.C.R., Novak, D.: A time-domain model for high-speed quantum-well lasers including carrier transport effects. IEEE J. Sel. Top. Quantum Electron. **1**(2), 494–504 (1995)
Schneider, H., Klitzing, K.V.: Thermionic emission and Gaussian transport of holes in a GaAs/Al GaAs multiple-quantum-well structure. Phys. Rev. B **38**(9), 6160–6165 (1988)
Shastri, B.J., Chen, C., Choquette, K.D., Plant, D.V.: Circuit modeling of carrier–photon dynamics in composite-resonator vertical-cavity lasers. IEEE J. Quantum Electron. **47**(12), 1537–1546 (2011)
Shchukin, V., Schöll, E., Kratzer, P.: Semiconductor Nanostructures. Springer, Berlin (2008)
Sugawara, M.: Semiconductor and Semimetals. Academic, New York (1999)
Sugawara, M., Hatori, N., Ebe, H., Ishida, M., Arakawa, Y., Akiyama, T., Otsubo, K., Nakata, Y.: Modeling room-temperature lasing spectra of 1.3-μm self-assembled InAs/GaAs quantum-dot lasers: homogeneous broadening of optical gain under current injection. J. Appl. Phys. **97**(4), 043523–043528 (2005)
Tong, C.Z., Yoon, S.F., Ngo, C.Y., Liu, C.Y., Loke, W.K.: Rate equations for 1.3-μm dots-under-a-well and dots-in-a-well self-assembled InAs–GaAs quantum-dot lasers. IEEE J. Quantum Electron. **42**(11), 1175–1183 (2006)
Tong, C.Z., Xu, D., Yoon, S.F.: Carrier relaxation and modulation response of 1.3-μm InAs–GaAs quantum dot lasers. J. Lightwave Technol. **27**(23), 5442–5450 (2009a)
Tong, C.Z., Xu, D.W., Yoon, S.F., Ding, Y., Fan, W.J.: Temperature characteristics of 1.3-μm p-doped InAs–GaAs quantum-dot vertical-cavity surface-emitting lasers. IEEE J. Sel. Top. Quantum Electron. **15**(3), 743–748 (2009b)
Tsou, B.P.C., Pulfrey, D.L.: A versatile SPICE model for quantum-well lasers. IEEE J. Quantum Electron. **33**(2), 246–254 (1997)
Wilmsen, C.W., Temkin, H., Coldren, L.A.: Vertical-Cavity Surface-Emitting Lasers. Cambridge Univ. Press, Cambridge (1999)
Xu, D.W., Yoon, S.F., Tong, C.Z.: Self-consistent analysis of carrier confinement and output power in 1.3-μm InAs–GaAs quantum-dot VCSELs. IEEE J. Quantum Electron. **44**(9), 879–885 (2008)
Yavari, M.H., Ahmadi, V.: Circuit-level implementation of semiconductor self-assembled quantum dot laser. IEEE J. Sel. Top. Quantum Electron. **15**(3), 774–779 (2009)
Yavari, M.H., Ahmadi, V.: Effects of carrier relaxation and homogeneous broadening on dynamic and modulation behavior of Self-assembled quantum dot laser. IEEE J. Sel. Top. Quantum Electron. **17**(5), 1153–1157 (2011)
Yu, S.F., Wong, W.N., Shum, P., Li, E.H.: Theoretical analysis of modulation response and second-order harmonic distortion in vertical-cavity surface-emitting lasers. IEEE J. Quantum Electron. **32**(12), 2139–2147 (1996)
Zory, P.S., Liao, P.F., Kelley, P.: Quantum Well Lasers. Academic Press, New York (1993)